ChemEurJ

Research Article
doi.org/10.1002/chem.202502463

Chemistry Europe
European Chemical Societies Publishing

www.chemeurj.org

Effects of Peripheral Substituents on the Optical and Electrochemical Properties of Dibenzo-5,10,15-triazaporphyrins

Kaori Kuwabara,[a] Uta Sakamaki,[b] Taiyou Tsutsumi,[c] Yui Wakasa,[d] Soji Shimizu,*[c] Mao Minoura,[d] Yoshifumi Kimura,[b] Haruyuki Nakano,[e] and Yoshihiro Matano*[f]

In contrast to the great advances of phthalocyanine-based materials, the potential of 5,10,15-triazaporphyrins has not been realized because of the lack of fundamental information about their structure-property relationships. Here, we report new derivatives of dibenzo-5,10,15-triazaporphyrin (DBTriAP) with aryl or alkyl substituents at the *meso* and/or β positions. Freebases of DBTriAP were prepared by the condensation of two types of 1,9-dibromodipyrrins with 1,3-diiminoisoindoline and subsequent functionalization of the β-pyrrolic carbons. Zinc(II) complexes of DBTriAP were obtained by complexation of the corresponding freebases with zinc(II) acetate. The optical and electrochemical properties of the DBTriAP derivatives were studied by steady-state and transient ultraviolet/visible absorption/emission spectroscopy, magnetic circular dichroism spectroscopy, cyclic voltammetry (CV), and density functional theory (DFT) calculations. Replacing the β-pyrrolic hydrogens of the 5-mesityl-DBTriAP derivatives with aryl groups resulted in substantial red shifts of the low-energy absorption band because of the effective π-delocalization and/or charge-transfer interaction with the DBTriAP chromophore. The 2,3,17,18-tetraethyl-DBTriAP freebase exhibited split redox processes in its cyclic voltammogram, suggesting the rapid formation of a π-stacked dimer radical cation facilitated by the highly planar structure. Most of the DBTriAP derivatives emitted red fluorescence with quantum yields of 0.07–0.31, indicating their potential as luminescent materials.

1. Introduction

Tetrabenzoazaporphyrins, in which one, two, or three *meso* methine units of tetrabenzoporphyrin (TBP) are replaced with nitrogen atoms, are hybrids of TBP and phthalocyanine. The fundamental properties of tetrabenzoazaporphyrins vary dramatically depending on the number of *meso* nitrogen (N_{meso}) atoms.[1–4] Tetrabenzotriazaporphyrin (TBTriAP), which contains three N_{meso} atoms, has C_{2v}-symmetry and is therefore polarized, unlike D_{4h}-symmetric TBP and phthalocyanine. The fundamental properties of TBTriAP are distinct from those of TBP.[5–19] The Q bands of TBTriAP are substantially red-shifted and more intense than those of TBP, reflecting the electronic effects of the N_{meso} atoms on the frontier orbitals of porphyrin. In addition, TBTriAP exhibits higher oxidation resistance and stronger electron-accepting ability than TBP because of its energetically stabilized highest occupied molecular orbital (HOMO) and lowest unoccupied molecular orbital (LUMO).

Several groups have used TBTriAP derivatives in the field of materials chemistry.[20–25] For example, Ozaki et al. reported the photovoltaic performances of bulk-heterojunction organic solar cells containing nonperipherally substituted octaalkyl-TBTriAP derivatives[21–23] as hole-transporting materials, and Ray and colleagues used solution-processed TBTriAP films in organic field-effect transistors.[24] By contrast, little information is available on triazaporphyrin (TriAP) derivatives with nonfused pyrrole units because of the lack of convenient methods for their synthesis and regiospecific diversification at their periphery. In general, TBTriAP derivatives have been prepared by condensation reactions of phthalonitrile and its derivatives with Grignard reagents, followed by chromatographic separation. However, this method is not suitable for the synthesis of nonfused and partially benzo-fused derivatives of TriAP. In 2012, Shimizu et al. reported a convenient method for the synthesis of nonfused TriAP **P1**, dibenzo-5,10,15-triazaporphyrin (DBTriAP)

[a] *K. Kuwabara*
Department of Fundamental Sciences, Graduate School of Science and Technology, Niigata University, Nishi-ku, Niigata 950-2181, Japan

[b] *U. Sakamaki, Prof. Y. Kimura*
Department of Molecular Chemistry and Biochemistry, Faculty of Science and Engineering, Doshisha University, Kyotanabe 610-0321, Japan

[c] *T. Tsutsumi, Prof. S. Shimizu*
Department of Applied Chemistry, Graduate School of Engineering and Center for Molecular Systems (CMS), Kyushu University, Nishi-ku, Fukuoka 819-0395, Japan
E-mail: ssoji@cstf.kyushu-u.ac.jp

[d] *Y. Wakasa, Prof. M. Minoura*
Department of Chemistry, College of Science, Rikkyo University, Toshima-ku, Tokyo 171-8501, Japan

[e] *Prof. H. Nakano*
Department of Chemistry, Graduate School of Science, Kyushu University, Nishi-ku, Fukuoka 819-0395, Japan

[f] *Prof. Y. Matano*
Department of Chemistry, Faculty of Science, Niigata University, Nishi-ku, Niigata 950-2181, Japan
E-mail: matano@chem.sc.niigata-u.ac.jp

Supporting information for this article is available on the WWW under https://doi.org/10.1002/chem.202502463

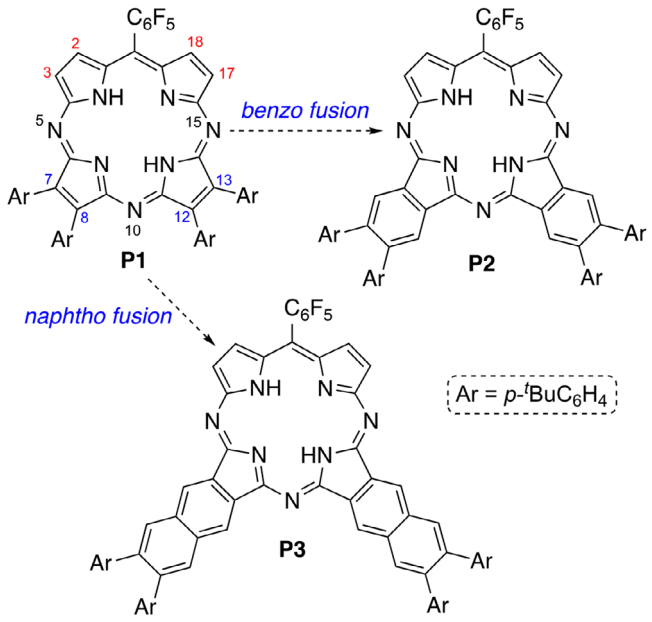

Figure 1. Structures of TriAP derivatives **P1**, **P2**, and **P3**.

P2, and dinaphtho-5,10,15-triazaporphyrin **P3** (Figure 1) from 5-pentafluorophenyl-1,9-dibromodipyrrin and the corresponding 1,3-diiminoisoindoline precursors.[26] They also studied the effect of the substituents attached at the 7, 8, 12, and 13 positions on the optical properties of the whole TriAP π-electron system, elucidating that the intramolecular charge transfer (ICT) transition strongly contributes to the long-wavelength absorption bands of the naphtho-fused derivative **P3**. These results highlight that chemical modification of the β-pyrrolic positions is a promising strategy to diversify the optical properties of the TriAP chromophore. However, the influence of the peripheral substituents at the 2, 3, 17, and 18 positions of TriAP on its optical and electrochemical properties has not been investigated.

Here we report freebases and Zn^{II} complexes of DBTriAP with aryl or ethyl groups at these positions. The optical and electrochemical properties of these new derivatives of DBTriAP are studied by steady-state and transient ultraviolet/visible (UV/Vis) absorption/emission spectroscopy, magnetic circular dichroism (MCD) spectroscopy, cyclic voltammetry (CV), and density functional theory (DFT) calculations.

2. Results and Discussion

2.1. Synthesis

Scheme 1 illustrates the synthesis of freebases and Zn^{II} complexes of 5-mesityl-DBTriAP (mesityl = 2,4,6-trimethylphenyl). Following a reported procedure,[26] a mixture of 1,9-dibromo-5-mesityldipyrrin **1**, 1,3-diiminoisoindoline, *N*-ethyldiisopropylamine, and *N*-methyl-2-pyrrolidone (NMP) was heated at 130 °C, affording freebase $\mathbf{2H_2}$ in 15% yield. Attempts to increase the yield of $\mathbf{2H_2}$ by changing the reaction conditions were unsuccessful because of the inevitable formation of

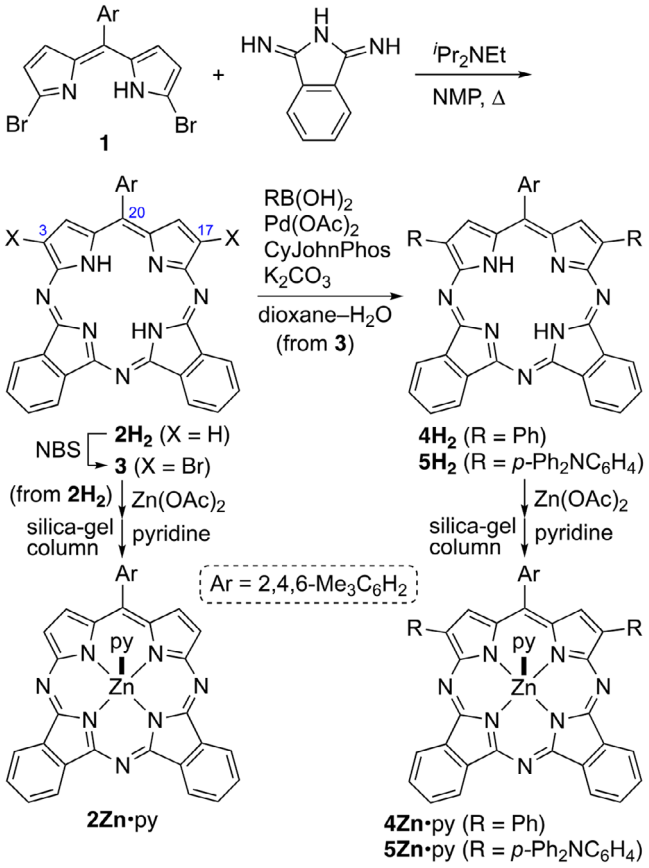

Scheme 1. Synthesis of **2M**, **3**, **4M**, and **5M**: M = H_2, Zn•py. py = pyridine.

unidentified products. Regioselective bromination of $\mathbf{2H_2}$ with *N*-bromosuccinimide (NBS) in CH_2Cl_2 yielded 3,17-dibromo-20-mesityl-DBTriAP **3**. Suzuki-Miyaura coupling of **3** with phenylboronic acid and *p*-(diphenylamino)phenylboronic acid in the presence of $Pd(OAc)_2$, 2-biphenyldicyclohexylphosphine (CyJohnPhos), and K_2CO_3 in boiling dioxane–H_2O afforded the corresponding 3,17-diaryl-5-mesityl-DBTriAPs $\mathbf{4H_2}$ and $\mathbf{5H_2}$, respectively. Treatment of $\mathbf{2H_2}$, $\mathbf{4H_2}$, and $\mathbf{5H_2}$ with $Zn(OAc)_2$ in $CHCl_3$—MeOH, followed by chromatographic separation with pyridine-containing eluents, furnished the corresponding Zn^{II} complexes **2Zn**•py, **4Zn**•py, and **5Zn**•py, respectively, as pyridine adducts.

Scheme 2 depicts the synthesis of the freebase and Zn^{II} complex of 2,3,17,18-tetraethyl-DBTriAP. The condensation of 1,9-dibromo-2,3,7,8-tetraethydipyrrin **6** with three equivalents of 1,3-diiminoisoindoline in NMP afforded freebase $\mathbf{7H_2}$, which was then converted to Zn^{II} complex **7Zn** by treatment with $Zn(OAc)_2$. This Zn^{II} complex was also isolated as a pyridine adduct through chromatographic separation with pyridine-containing eluents.

The newly prepared compounds were characterized by NMR spectroscopy and high-resolution mass spectrometry. The physical properties of the Zn^{II} complexes were measured in the presence of pyridine to improve solubility. The ^1H NMR spectra of all derivatives exhibited the diamagnetic ring current effect on the peripheral protons. For example, β-CH signals of $\mathbf{2H_2}$ and **2Zn**•py were observed in the range of 8.77–8.32 ppm, whereas *meso*-CH signals of $\mathbf{7H_2}$ and **7Zn**•py were observed at 9.61 and

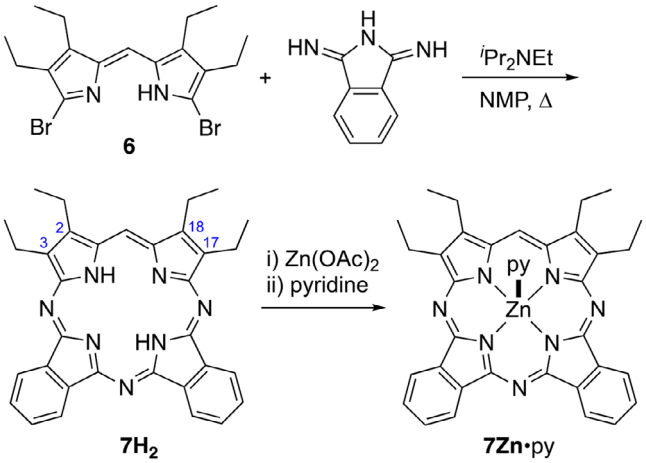

Scheme 2. Synthesis of $7H_2$ and 7Zn•py. py = pyridine.

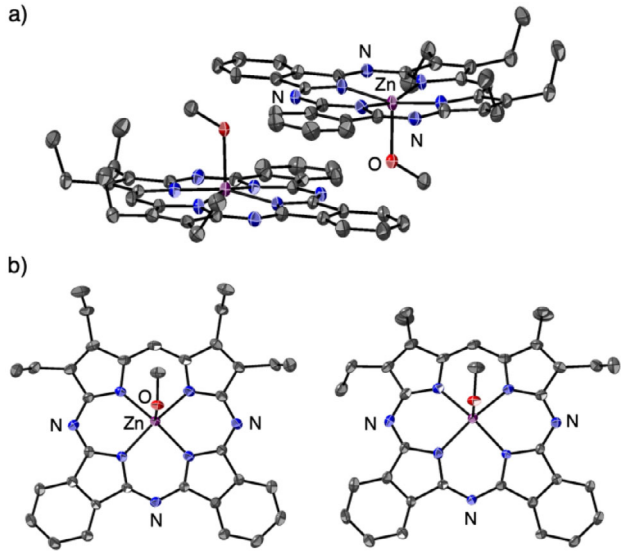

Bond lengths (Å)		Bond lengths (Å)	
Zn–N	1.999(3)–2.026(4)	Zn–N	2.000(3)–2.029(4)
Zn–O	2.103(3)	Zn–O	2.093(3)
N_{meso}–C_α	1.316(5)–1.355(6)	N_{meso}–C_α	1.315(5)–1.356(6)
C_{meso}–C_α	1.401(5)–1.407(7)	C_{meso}–C_α	1.390(7)–1.402(5)

Figure 2. ORTEP diagrams (50% probability ellipsoids) and selected bond lengths of 7Zn•MeOH. Hydrogen atoms are omitted for clarity. a) Side view of a pair of two independent molecules. b) Top views of two independent molecules.

9.75 ppm, respectively. The inner NH signals of the freebases were not clearly observed, suggesting that the rate of exchange between the two NH tautomers is close to the NMR time scale. Increasing the concentration of a $CDCl_3$ solution of $7H_2$ from 3 to 11 mM caused a slight upfield shift ($\Delta\delta = +0.33$ ppm) of the *meso*-CH signal, indicating that $7H_2$ aggregated at the relatively high concentration (Figure S1 in the Supporting Information).

The axial pyridine ligand of 7Zn•py was removed by the treatment with an aqueous HCl solution. The resulting solid was sparingly soluble in CH_2Cl_2 and $CHCl_3$, but somewhat soluble in these solvents in the presence of a small amount of MeOH. The structure of the MeOH adduct of **7Zn** was unambiguously elucidated by X-ray crystallography. Figure 2 shows the crystal structure and selected bond lengths of 7Zn•MeOH, and Figure S1 displays supplementary details. The unit cell contains two independent π–π stacked molecules with interplanar π–π distances of approximately 3.4–3.5 Å. The structure contains complementary hydrogen-bonding interactions between the hydroxy groups of the axial MeOH ligands and N_{meso} atoms. The orientation of the peripheral ethyl groups is (*up*,*up*,*up*,*up*) in one molecule, and (*up*,*up*,*up*,*down*) in the other. In each molecule, the zinc center has a square pyramidal geometry and deviates from the core-N_4 plane by 0.305–0.384 Å because of the axial coordination of the MeOH molecule. The N_{meso}—C_α bond lengths (1.315–1.356 Å) are appreciably shorter than the C_{meso}—C_α bond lengths (1.390–1.407 Å), reflecting the difference in covalent bond radii of C and N atoms. The Zn—O bond distances (2.093–2.103 Å) are longer than the sum of their covalent radii (1.86 Å) but considerably shorter than their van der Waals radii (ca. 2.9 Å), indicating that MeOH bonds strongly to the zinc center in the solid state. Both molecules exhibit highly planar DBTriAP rings with root-mean-square deviations (Δd_{RMS}) of 0.044–0.087 Å.

2.2. Optical and Photophysical Properties

The UV/Vis absorption spectra of the DBTriAP derivatives in CH_2Cl_2 are shown in Figure 3a, and their absorption maxima (λ_{max}) are summarized in Table 1. Compounds $2H_2$ and 2Zn•py exhibited Q bands in the range of 500–650 nm with the λ_{max} values of 623/582 and 610/598 nm, respectively, whereas 2,3,17,18-tetraethyl-DBTriAP derivatives $7H_2$ and 7Zn•py showed Q bands in a similar range with the λ_{max} values of 640/594 and 624/607 nm, respectively. The Q bands of **4M** (λ_{max} = 648/607 for $4H_2$ and 624 nm for 4Zn•py) were red-shifted from those of **2M**, suggesting that introducing two phenyl groups at the 3 and 17 positions extended π-conjugation and led to narrowing of the HOMO–LUMO gap. The TPA-appended derivatives $5H_2$ and 5Zn•py (TPA = triphenylamine) exhibited further red-shifted, broadened absorption bands with λ_{max} of 670 and 651 nm, respectively, reflecting the strong influence of the TPA units on the optical properties of these compounds (vide infra).

DFT and time-dependent DFT (TD-DFT) calculations of **2M**, $4H_2$, $5H_2$, and **7M-m** (the peripheral ethyl groups of **7M** were replaced with methyl groups) enabled the assignment of the observed electronic transitions (Figure 4 and Table S1). The involvement of three N_{meso} atoms meant that the four porphyrin-derived orbitals (a_{1u}/a_{2u} and e_{gx}/e_{gy}) were nondegenerate for all DBTriAP derivatives. Among them, the a_{1u}-type HOMOs have relatively large orbital coefficients on the 2, 3, 17, and 18 positions, so their energies are strongly influenced by the β-substituents. The TD-DFT calculations revealed that the intense Q bands of **2M**, $4H_2$, and **7M** in the range of 500–700 nm are composed of the DBTriAP-centered, HOMO-to-LUMO, and HOMO-to-LUMO+1 transitions. In the case of $4H_2$, the peripheral phenyl groups are π-conjugated with the TriAP ring, resulting in a narrower HOMO–LUMO gap than that of $2H_2$. In the case of **7M-m**, the

Table 1. Optical and photophysical data for DBTriAP derivatives in CH_2Cl_2.[a]

Compd	λ_{abs} /λ_{em} [nm]	Φ_f	τ_f [ns]	k_r [s^{-1}]	k_{nr} [s^{-1}]
$2H_2$	568, 582, 623/632	0.27	5.53	4.9×10^7	1.3×10^8
$4H_2$	607, 648/658	0.23	4.44	5.2×10^7	1.7×10^8
$5H_2$	532, 670/760	<0.01	n.d.	n.d.	n.d.
$7H_2$	577, 594, 640/646	0.31	5.48	5.7×10^7	1.3×10^8
2Zn•py	551, 598, 610/617	0.15	2.13	7.0×10^7	4.0×10^8
4Zn•py	624, 631/647	0.12	1.79	6.7×10^7	4.9×10^8
5Zn•py	543, 651/774	0.037	n.d.	n.d.	n.d.
7Zn•py	607, 624/629	0.065	2.63	2.5×10^7	3.6×10^8

[a] λ_{abs}: Absorption maxima (>500 nm). λ_{em}: Fluorescence maxima. Φ_f: Absolute fluorescence quantum yields. τ_f: Fluorescence lifetimes. k_r: radiative decay rate constants. k_{nr}: nonradiative decay rate constants.

four methyl groups destabilize the HOMO to a greater extent than the LUMO, resulting in a narrower HOMO–LUMO gap than those of **2M** (M = H_2, Zn). Therefore, the red shifts of the Q-like bands observed for **$4H_2$** and **7M** can be attributed to the efficient π-conjugation with phenyl groups and the inductive effect of the ethyl groups, respectively. The HOMO of **$5H_2$** was composed of a TPA π orbital and DBTriAP-derived a_{1u}-type orbital, and the HOMO−1 was a pure TPA π orbital. These TPA-based HOMOs are located at higher energy than the DBTriAP-derived HOMO−2. In contrast, the LUMO and LUMO+1 of **$5H_2$** are typical DBTriAP π orbitals. The low-energy π–π* transitions of **$5H_2$** are composed of excitations from the HOMO/HOMO−1 to the LUMO/LUMO+1, indicating that the broad transitions of **$5H_2$** and **5Zn** in the range of 600–750 nm are caused by ICT from the TPA units to the DBTriAP chromophore.

To gain deeper insight into the effect of the peripheral substituents on the absorption bands of the DBTriAP derivatives, we carried out MCD measurements of **2M**, **$4H_2$**, **$5H_2$**, and **7M** in CH_2Cl_2 (Figure 5). MCD spectroscopy provides valuable information about the electronic structure of porphyrins and related compounds, which is complementary to that obtained by UV/vis absorption spectroscopy.[27,28] Faraday *B* terms, which are Gaussian-shaped signals with similar spectral profiles to those of the absorption bands, irrespective of their signs, were exclusively observed for the Soret and Q bands in all cases. For example, the MCD spectrum of **2Zn•py** exhibited Faraday *B* terms with negative and positive envelopes at 612 and 597 nm, corresponding to the split Q-band absorption at 610 and 598 nm (Figure 5b). A couple of Faraday *B* terms are caused by the field-induced mixing of nondegenerate transitions as a second-order effect. Because the Soret and Q bands of the DBTriAP derivatives, except for **$5H_2$** mainly consist of the HOMO−1 (HOMO−2 for **$4H_2$** and **$7H_2$-m**)-to-LUMO/LUMO+1 transitions and the HOMO-to-LUMO/LUMO+1 transitions, respectively, as predicted by the TD-DFT calculations, the observed Faraday *B* terms indicate the nondegeneracy of these frontier molecular orbitals (MOs).

The sign sequence of the Faraday *B* terms also provides information about the magnitude relationship between the splitting energy of the HOMO and HOMO−1 (ΔHOMO = $E_{HOMO} - E_{HOMO-1}$) and that of the LUMO and LUMO+1 (ΔLUMO = $E_{LUMO+1} - E_{LUMO}$). A minus-to-plus sign sequence in ascending energy corresponds to ΔHOMO > ΔLUMO, whereas a plus-to-minus sign sequence corresponds to ΔLUMO > ΔHOMO. Therefore, the minus-to-plus sign sequences observed for the Soret and Q bands of all compounds indicate ΔHOMO > ΔLUMO for these DBTriAP derivatives. This relationship was reproduced by the DFT calculations (Figure 4). The magnitude of the Q-band splitting energy estimated from the peak positions of the negative and positive envelopes was greater for the freebases than the corresponding Zn^{II} complexes, reflecting the lower molecular symmetry of the freebases. Despite the broad absorption in the Q-band region, the Faraday *B* terms of **$5H_2$** at 680 and 637 nm indicate their origin is Q bands. The extensive broadening compared with that of other DBTriAP derivatives is ascribed to the presence of ICT bands. This assignment is consistent with the theoretical absorption of **$5H_2$** obtained from the TD-DFT calculation. The theoretical absorption in the Q-band region contains ICT transitions from the TPA-derived MOs (HOMO and HOMO−1) to the DBTriAP-centered LUMO and LUMO+1 and Q-band transitions from the DBTriAP-centered MOs (HOMO and HOMO−2) to the LUMO and LUMO+1.

As shown in Figure 3b, **2M**, **4M**, and **7M** in CH_2Cl_2 emit red fluorescence with absolute quantum yields (Φ_f) of 0.23–0.31 for the freebases and 0.07–0.15 for the Zn^{II} complexes. Stokes shifts of **2M** and **7M** were determined to be 130–230 cm^{-1}, reflecting the rigid π-framework of the DBTriAP chromophore. In contrast to **2M** and **4M**, **5M** was weakly fluorescent or almost nonfluorescent. To further investigate the excited-state dynamics of the DBTriAP derivatives, fluorescence lifetimes (τ_f) of **2M**, **4M**, and **7M** in CH_2Cl_2 were measured by time-resolved fluorescence spectroscopy (Table 1). The fluorescence decay profiles of these compounds were well simulated by a single-exponential function with τ_f of 4.44–5.53 ns for the freebases and 1.79–2.63 ns for the Zn^{II} complexes. The radiative and nonradiative rate constants (k_r and k_{nr}, respectively), obtained from τ_f and Φ_f, are summarized in Table 1. The Φ_f values of the Zn^{II} complexes are smaller than those of the corresponding freebases because of the larger increase of k_{nr} than k_r upon complex formation. The substitution of the β-pyrrolic hydrogen atoms with phenyl groups (**4M** vs. **2M**) led to a slight decrease of Φ_f, which was attributed to an increase of k_{nr}. These findings suggest that the rotation of the

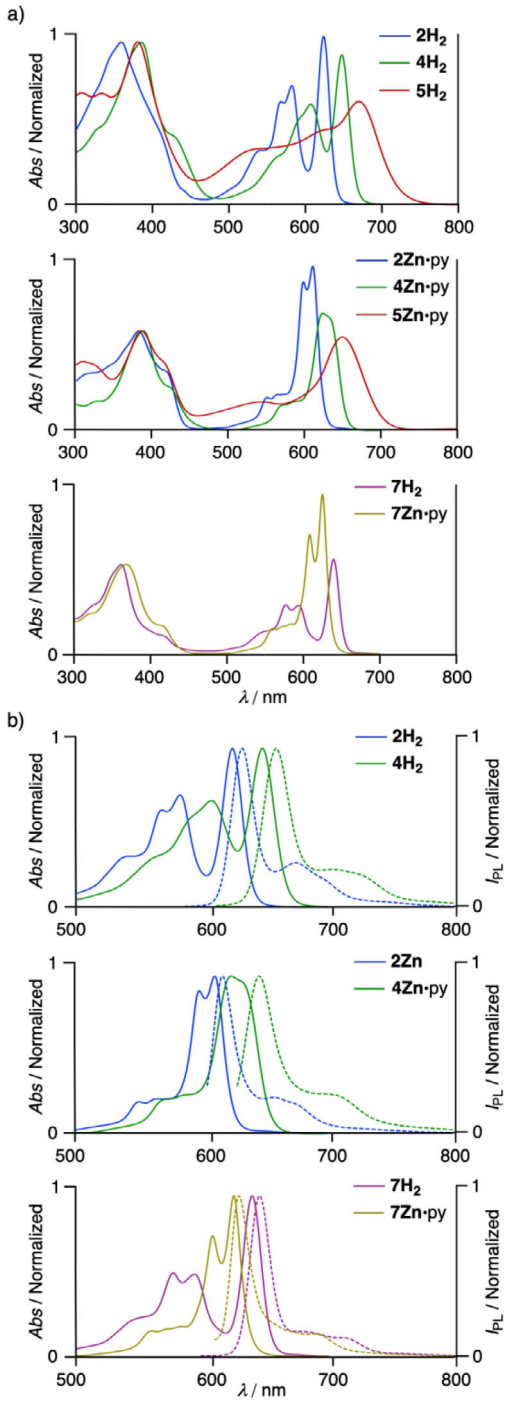

Figure 3. UV/Vis absorption spectra of a) **2M**, **4M**, **5M**, and **7M** in CH_2Cl_2. b) UV/Vis absorption/emission spectra of **2M**, **4M**, and **7M** in CH_2Cl_2. M = H_2, Zn•py.

axial pyridine ligand of the Zn^{II} complexes and the peripheral phenyl groups accelerates nonradiative decay from the singlet excited state.

2.3. Electrochemical Properties

The redox behavior of all DBTriAP derivatives in CH_2Cl_2 was measured by CV with Bu_4NPF_6 as a supporting electrolyte, as presented in Figure 6 with redox potentials (*E*). The electrochemical HOMO–LUMO gaps determined by CV were in good agreement with the optical HOMO–LUMO gaps determined by UV/Vis absorption spectroscopy. In both cases, the HOMO–LUMO gaps of **2M**, **4M**, and **5M** decreased in this order. The Zn^{II} complexes were easier to oxidize and more difficult to reduce than the corresponding freebases. The *E* values of 20-mesityl-DBTriAP derivatives **2M** were shifted to the positive side by 0.11–0.32 V compared with those of the corresponding 2,3,17,18-tetraethyl-DBTriAP derivatives **7M**. As predicted by the DFT calculations, replacing the β-pyrrolic hydrogens with phenyl groups shifted the DBTriAP-centered $18\pi/17\pi$ and $18\pi/19\pi$ redox couples to the negative and positive directions, respectively. In contrast, introducing two TPA units at the β positions caused cathodic shifts of the TPA-centered oxidation processes.

The split redox couples exhibited by the compounds are worth noting. In the cyclic voltammograms of **5M**, the TPA-centered oxidation processes were observed at +0.33 V (1e) and +0.47 V (1e) for $\mathbf{5H_2}$ and +0.22 V (1e) and +0.44 V (1e) for **5Zn•**py, suggesting that an unshared electron spin was delocalized over the two TPA moieties in their cation radicals. The cyclic voltammogram of $\mathbf{7H_2}$ also exhibited split redox couples at +0.35 V (1e) and +0.61 V (1e). At the concentration of the CV measurement (ca. 1 mM), an electrochemically generated radical cation of $\mathbf{7H_2}$ is likely to aggregate with a neutral molecule to form a π-stacked dimer radical cation on the electrode surface, as reported for TBTriAP derivatives.[11] In contrast, no aggregation behavior was observed for $\mathbf{2H_2}$, probably because of the steric hindrance of the mesityl group attached at the 20 position.

3. Conclusions

Freebases of 20-mesityl- and 2,3,17,18-tetraethyl-DBTriAP were prepared by one-pot condensation reactions of the corresponding 2,9-dibromodipyrrins with 1,3-diiminoisoindoline. Aryl groups were introduced onto the β-pyrrolic carbons of the 20-mesityl derivative by Suzuki-Miyaura coupling reactions with arylboronic acids. Zn^{II} complexes were prepared by metalation of the freebases with $Zn(OAc)_2$. Attaching phenyl groups at the 3 and 17 positions of 20-mesityl-DBTriAP caused red shifts of the Q bands originating from the porphyrin-centered π–π^* transitions because of the extended π-conjugation with the peripheral phenyl substituents. Introducing *p*-(diphenylamino)phenyl groups at these positions resulted in obvious red shifts of the UV/Vis absorption bands caused by the ICT transition from the electron-donating TPA units to the electron-accepting DBTriAP chromophore. The freebase of 2,3,17,18-tetraethyl-DBTriAP exhibited concentration-dependent changes in its NMR spectra, reflecting the aggregation behavior of the planar DBTriAP π-electron system. Most of the DBTriAP derivatives emitted fluorescence with Φ_f of 0.07–0.31 and τ_f of 1.8–5.5 ns. The present study provides valuable information for understanding the intrinsic effects of the peripheral substituents on the optical and electrochemical properties of TriAP-based π-electron systems and paves the way for developing new azaporphyrin-based materials.

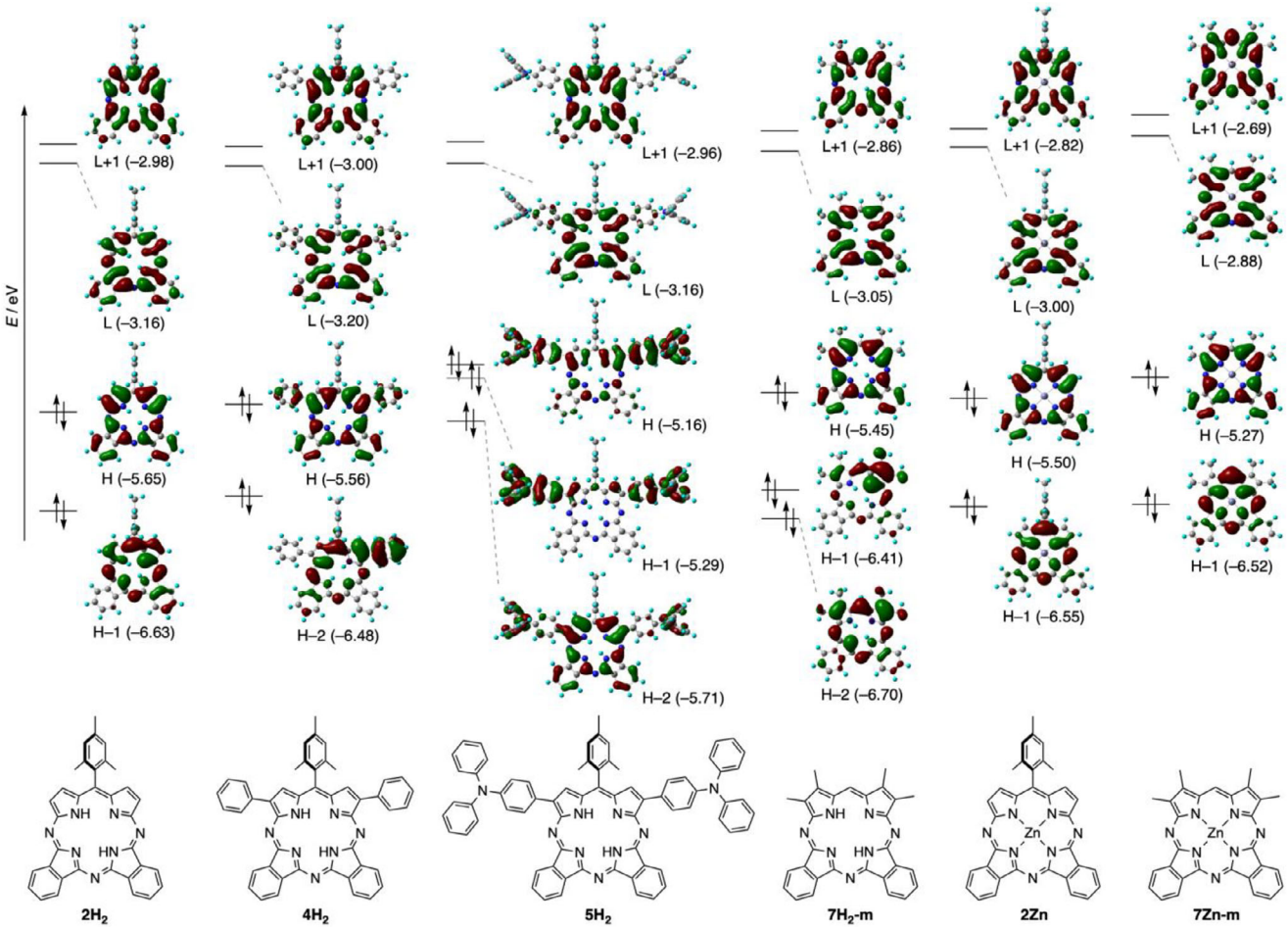

Figure 4. Selected Kohn-Sham orbitals and their energies of **2H$_2$**, **4H$_2$**, **5H$_2$**, **7H$_2$-m**, **2Zn**, and **7Zn-m** calculated by the DFT method.

4. Experimental Section

General Remarks: All melting points were recorded on a micro melting point apparatus and are uncorrected. The NMR spectra were recorded on 400 MHz and 700 MHz (Agilent and Bruker) spectrometers. The ^{1}H and ^{13}C chemical shifts are reported in ppm as relative values versus tetramethylsilane. High-resolution mass (HRMS) spectra were measured on a Bruker solarix FT-ICR (Matrix Assisted Laser Desorption/Ionization; MALDI) spectrometer. The matrix used for MALDI was *trans*-2-[3-(4-*tert*-butylphenyl)-2-methyl-2-propenylidene]malononitrile (DCTB) or a mixture of DCTB and sodium trifluoroacetate (NaTFA). The steady-state UV/Vis absorption spectra were measured on a JASCO V-730 or V-770 spectrophotometer, and the UV/Vis fluorescence spectra were measured on a JASCO EP-8300 spectrophotometer. Absolute fluorescence quantum yields were measured on a Hamamatsu Photonics Quantaurus-QY spectrometer. Redox potentials and electrochemical behavior were measured at room temperature on an ALS model 650E electrochemical workstation using a glassy carbon working electrode, a platinum wire counter electrode, and an Ag/Ag^{+} [0.01 M $AgNO_3$, 0.1 M Bu_4NPF_6 (MeCN)] reference electrode. Thin-layer chromatography was performed with Kieselgel 60 F254, and preparative column chromatography was performed using Silica Gel 60 spherical, neutrality. All reactions were performed under an argon atmosphere. Compound **1** was prepared according to a reported procedure.[29] Other chemicals and solvents were of reagent grade quality and used without further purification unless otherwise noted. For all the synthesis and characterization data of new compounds are reported in the Supporting Information.

X-ray Crystallographic Analysis: Single crystals of **7Zn**•MeOH used for the measurements were grown from $CHCl_3$—MeCN—MeOH at room temperature. Deposition Number 2476447 contains the supplementary crystallographic data for this paper. These data are provided free of charge by the joint Cambridge Crystallographic Data Centre and Fachinformationszentrum Karlsruhe http://www.ccdc.cam.ac.uk/structures Access Structures service. Selected parameters are as follows. $C_{34}H_{33}N_7OZn$, MW = 621.04, 0.010 × 0.010 × 0.010 mm, triclinic, *P*−1, a = 13.931(13) Å, b = 14.181(14) Å, c = 16.011(15) Å, α = 101.202(12)°, β = 104.387(11)°, γ = 99.386(13)°, V = 2930(5) Å^3, Z = 4, ρ = 1.408 g cm^{-3}, μ = 2.13 cm^{-1}, collected 68 278, independent 13 421, parameters 785, R_w = 0.2041, R = 0.0606 ($I > 2\sigma(I)$), GOF = 0.950.

DFT Calculations: The geometries of **2H$_2$**, **4H$_2$**, **5H$_2$**, **5Zn**, **7H$_2$-m**, and **7Zn-m** were optimized with the DFT method. The basis sets used for the optimization were the 6–311G(d,p) basis set[30] for H, C, and N and the Wachters–Hay all-electron basis set[31–33] supplemented with one f-function (exponent: 1.62) for Zn. The functional of DFT was the Becke, three-parameter, Lee–Yang–Parr (B3LYP) exchange-correlation functional.[34,35] The optimized geometries were confirmed to be minima by vibrational analysis. The Cartesian coordinates and computed total energies are summarized in Table S2. The excitation energies and oscillator strengths listed in Table S1 were computed with the TD-DFT method. The solvent

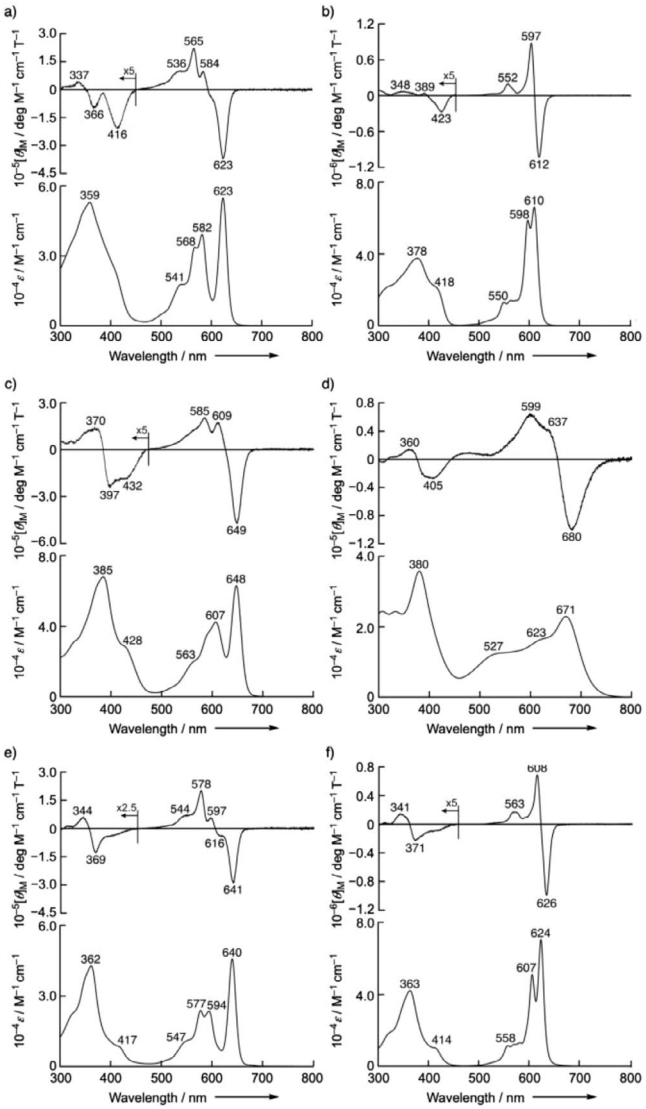

Figure 5. UV/Vis MCD (top) and absorption (bottom) spectra of a) **$2H_2$**, b) **2Zn•**py, c) **$4H_2$**, d) **$5H_2$**, e) **$7H_2$**, and f) **7Zn•**py in CH_2Cl_2.

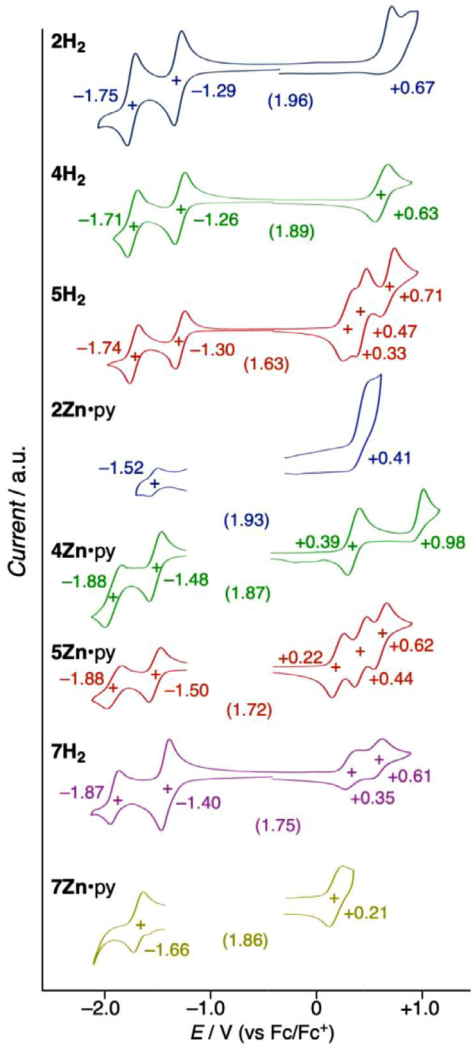

Figure 6. Cyclic voltammograms of **$2H_2$**, **$4H_2$**, **$5H_2$**, **2Zn•**py, **4Zn•**py, **5Zn•**py, **$7H_2$**, and **7Zn•**py; [DBTriAP] = ca. 1 mM. Measured in CH_2Cl_2 with Bu_4NPF_6 as a supporting electrolyte. Scan rate = 60 mV s^{-1}. Half-wave potentials for the reversible processes and peak potentials determined by differential pulse voltammetry for the irreversible processes are listed.

effects were incorporated in both the DFT and TD-DFT calculations using the polarizable continuum model (PCM) with the integral equation formalism variant.[36] All the calculations were carried out using the Gaussian 16 suite of programs.[37]

Magnetic Circular Dichroism Spectroscopy Measurements: Magnetic circular dichroism spectra were recorded on a JASCO J-1500 spectrodichrometer by applying parallel and antiparallel magnetic fields to the light propagation with a 1.6 T permanent magnet (T = tesla). The magnitudes were expressed in terms of molar ellipticity per tesla ($[\theta]_M$ / deg dm^3 mol^{-1} cm^{-1} T^{-1}).

Fluorescence Lifetime Measurements: The fluorescence lifetimes of **$2H_2$**, **$4H_2$**, **$7H_2$**, **2Zn•**py, **4Zn•**py, and **7Zn•**py were measured using a streak camera as a fluorescence detector. The excitation pulse (370 nm) was generated by taking the second harmonic pulse from the optical parametric amplifier (Spectra Physics, TOPAS-C) operated by the fundamental output of an amplified Ti:Sapphire laser system (Spectra Physics, Spitfire XPpro).

Acknowledgments

This work was supported by JSPS KAKENHI (23K23329 to YM, 21K04980 to HN) from MEXT, Japan. This study was supported by the Joint Usage/Research Center [JURC, Institute for Chemical Research (ICR), Kyoto University] by providing access to Bruker solarix spectrometer (FT-ICR). We would also like to express our gratitude to the SPring-8 synchrotron facility, where synchrotron-radiation experiments were performed at the BL02B1 beamlines with the approval of the Japan Synchrotron Radiation Research Institute (JASRI) under proposal numbers 2024A1948, 2024B1757, 2024B1931, and 2025A1830.

Conflict of Interest

The authors declare no conflict of interest.

Data Availability Statement

The data that support the findings of this study are available in the supplementary material of this article.

Keywords: aggregation · dyes/pigments · fluorescence · redox chemistry · triazaporphyrin

[1] K. Ishii, N. Kobayashi, in *The Porphyrin Handbook* Vol. *16*, (Eds.: K. M. Kadish, K. M. Smith, R. Guilard), Academic Press, San Diego, **2003**, pp. 1–42.
[2] J. Mack, N. Kobayashi, *Chem. Rev.* **2011**, *111*, 281, https://doi.org/10.1021/cr9003049.
[3] Y. Matano, *Chem. Rev.* **2017**, *117*, 3138, https://doi.org/10.1021/acs.chemrev.6b00460.
[4] A. V. As, C. C. Joubert, B. E. Buitendach, E. Erasmus, J. Conradie, A. N. Cammidge, I. Chambrier, M. J. Cook, J. C. Swarts, *Inorg. Chem.* **2015**, *54*, 5329, https://pubs.acs.org/doi/10.1021/acs.inorgchem.5b00380.
[5] J. H. Helberger, *Justus Liebigs Ann. Chem.* **1937**, *529*, 205, https://doi.org/10.1002/jlac.19375290114.
[6] J. H. Helberger, A. von Rebay, *Justus Liebigs Ann. Chem.* **1937**, *531*, 279, https://doi.org/10.1002/jlac.19375310109.
[7] P. A. Barrett, R. P. Linstead, G. A. P. Tuey, J. M. Robertson, *J. Chem. Soc.* **1939**, 1809, https://doi.org/10.1039/jr9390001809.
[8] P. A. Barrett, R. P. Linstead, F. G. Rundall, G. A. P. Tuey, *J. Chem. Soc.* **1940**, 1079, https://doi.org/10.1039/jr9400001079.
[9] E. A. Makarova, V. N. Kopranenkov, V. K. Shevtsov, E. A. Luk'yanets, *Chem. Heterocycl. Compd.* **1989**, *25*, 1159, https://doi.org/10.1007/BF00470696.
[10] C. C. Leznoff, N. B. McKeown, *J. Org. Chem.* **1990**, *55*, 2186, https://doi.org/10.1021/jo00294a038.
[11] Y. H. Tse, A. Goel, M. Hu, A. B. P. Lever, C. C. Leznoff, J. E. Van Lier, *Can. J. Chem.* **1993**, *71*, 742, https://doi.org/10.1139/v93-098.
[12] J. Mack, N. Kobayashi, C. C. Leznoff, M. J. Stillman, *Inorg. Chem.* **1997**, *36*, 5624. https://doi.org/10.1021/ic961389n.
[13] N. E. Galanin, E. V. Kudrik, G. P. Shaposhnikov, *Russ. J. Org. Chem.* **2002**, *38*, 1200, https://doi.org/10.1023/A:1020918030094.
[14] N. E. Galanin, L. A. Yakubov, E. V. Kudrik, G. P. Shaposhnikov, *Russ. J. Gen. Chem.* **2008**, *78*, 1436, https://doi.org/10.1134/S107036320807027X.
[15] E. M. Antunes, T. Nyokong, *J. Porphyrins Phthalocyanines* **2009**, *13*, 153, https://doi.org/10.1142/S1088424609000048.
[16] A. N. Cammidge, M. J. Cook, D. L. Hughes, F. Nekelson, M. Rahman, *Chem. Commun.* **2005**, 930, https://doi.org/10.1039/b414820g.
[17] A. N. Cammidge, I. Chambrier, M. J. Cook, D. L. Hughes, M. Rahman, L. S. Vargas, *Chem. Eur. J.* **2011**, *17*, 3136, https://doi.org/10.1002/chem.201002176.
[18] J. Mack, L. S. Vargas, S. J. Coles, G. J. Tizzard, I. Chabrier, A. N. Cammidge, M. J. Cook, N. Kobayashi, *Inorg. Chem.* **2012**, *51*, 12820, https://doi.org/10.1021/ic301712h.
[19] R. F. Theisen, L. Huang, T. Fleetham, J. B. Adams, J. Li, *J. Chem. Phys.* **2015**, *142*, 094310, https://doi.org/10.1063/1.4913757.
[20] K. Liou, M. Y. Ogawa, T. P. Newcomb, G. Quirion, M. Lee, M. Poirier, W. P. Halperin, B. M. Hoffman, J. A. Ibers, *Inorg. Chem.* **1989**, *28*, 3889, https://doi.org/10.1021/ic00319a026.
[21] Q.-D. Dao, T. Uno, M. Ohmori, K. Watanabe, H. Itani, A. Fujii, Y. Shimizu, M. Ozaki, *J. Phys. D: Appl. Phys.* **2015**, *48*, 385103, https://doi.org/10.1088/0022-3727/48/38/385103.
[22] Q.-D. Dao, A. Fujii, M. Ozaki, *Jpn. J. Appl. Phys.* **2016**, *55*, 03DB01, https://doi.org/10.7567/JJAP.55.03DB01.
[23] Q.-D. Dao, A. Fujii, H. Itani, Y. Shimizu, M. Ozaki, *Jpn. J. Appl. Phys.* **2020**, *59*, 101003, https://doi.org/10.35848/1347-4065/abb8b8.
[24] N. B. Chaure, A. N. Cammidge, I. Chambrier, A. K. Ray, *J. Appl. Phys.* **2018**, *124*, 235501, https://doi.org/10.1063/1.5055588.
[25] Q.-D. Dao, N.-A. Tran, T.-H. Doan, *Opt. Mater.* **2022**, *132*, 112820, https://doi.org/10.1016/j.optmat.2022.112820.
[26] S. Shimizu, Y. Ito, K. Oniwa, S. Hirokawa, Y. Miura, O. Matsushita, N. Kobayashi, *Chem. Commun.* **2012**, *48*, 3851, https://doi.org/10.1039/c2cc30625e.
[27] J. Mack, M. J. Stillman, N. Kobayashi, *Coord. Chem. Rev.* **2007**, *251*, 429, https://doi.org/10.1016/j.ccr.2006.05.011.
[28] N. Kobayashi, A. Muranaka, J. Mack, *Circular Dichroism and Magnetic Circular Dichroism Spectroscopy for Organic Chemists*, RSC, UK, **2011**, https://doi.org/10.1039/9781849732932.
[29] Y. Matano, T. Shibano, H. Nakano, H. Imahori, *Chem. Eur. J.* **2012**, *18*, 6208, https://doi.org/10.1002/chem.201200463.
[30] R. Krishnan, J. S. Binkley, R. Seeger, J. A. Pople, *J. Chem. Phys.* **1980**, *72*, 650, https://doi.org/10.1063/1.438955.
[31] A. J. H. Wachters, *J. Chem. Phys.* **1970**, *52*, 1033, https://doi.org/10.1063/1.1673095.
[32] P. J. Hay, *J. Chem. Phys.* **1977**, *66*, 4377, https://doi.org/10.1063/1.433731.
[33] K. Raghavachari, G. W. Trucks, *J. Chem. Phys.* **1989**, *91*, 1062, https://doi.org/10.1063/1.457230.
[34] C. Lee, W. Yang, R. G. Parr, *Phys. Rev. B* **1988**, *37*, 785, https://doi.org/10.1103/PhysRevB.37.785.
[35] A. D. Becke, *J. Chem. Phys.* **1993**, *98*, 5648, https://doi.org/10.1063/1.464913.
[36] E. Cancès, B. Mennucci, J. Tomasi, *J. Chem. Phys.* **1997**, *107*, 3032; https://pubs.aip.org/aip/jcp/article-abstract/107/8/3032/475611
[37] *Gaussian 16, Revision C.01*; M. J. Frisch, G. W. Trucks, H. B. Schlegel, G. E. Scuseria, M. A. Robb, J. R. Cheeseman, G. Scalmani, V. Barone, G. A. Petersson, H. Nakatsuji, X. Li, M. Caricato, A. V. Marenich, J. Bloino, B. G. Janesko, R. Gomperts, B. Mennucci, H. P. Hratchian, J. V. Ortiz, A. F. Izmaylov, J. L. Sonnenberg, D. Williams-Young, F. Ding, F. Lipparini, F. Egidi, J. Goings, B. Peng, A. Petrone, T. Henderson, D. Ranasinghe, et al., Gaussian, Inc., Wallingford CT, **2019**.

Manuscript received: August 3, 2025
Revised manuscript received: October 4, 2025
Version of record online: October 24, 2025